uncertainties. Also in Fig. 2, the cross sections predicted from the Bertini program are shown. The calculated results are extracted in the same ranges of polar angle as for the experiment. Therefore, it is concluded that at both forward and large angles, the proton spectra decrease rapidly with increasing energy and that the experimental results are in reasonable agreement with the Monte Carlo calculation.

Study of the Reactions Cd(Ar⁴⁰, xn)Dy†

Joseph B. Natowitz

Department of Chemistry and Cyclotron Institute, Texas A&M University, College Station, Texas 77840

AND

John M. Alexander*

Department of Chemistry, State University of New York, Stony Brook, New York 11790

(Received 29 July 1969)

Excitation functions are reported for the reactions of Cd^{114} and Cd^{116} with Ar^{40} to produce Tb^{149}, Dy^{150}, and Dy^{151}. Range measurements in Al for the recoiling Dy products indicate that compound-nucleus formation is the first step in the reaction. From the cross sections, it is concluded that the angular momentum spectrum for the reactions $Cd(Ar^{40}, 6n$ and $7n)$ is very similar to that for $(Ne^{20}, 6n$ and $7n)$ reactions. The range measurements extend the span of experimental range-energy information for these nuclei from 4 to 60 MeV. These range data expressed in terms of fractional effective charge $[\gamma = Z_{eff}/Z]$ are found to correlate well with data for $Br^{79,80}$, I^{127}, and fission fragments.

I. INTRODUCTION

THE production of Tb^{149}, Dy^{150}, and Dy^{151} nuclei by (HI, xn) reactions has been extensively studied with projectiles as massive as Ne^{22}.[1–5] In the present paper, we report the measurement of excitation functions and ranges in Al for Tb^{149}, Dy^{150}, and Dy^{151} produced by (Ar^{40}, xn) reactions with Cd^{114} and Cd^{116}. Similar measurements have been reported by Kumpf and Karnaukhov[6] who used the internal beam of the Dubna cyclotron. Comparison of these excitation functions with those for $(C^{12}, 6n$ or $7n)$ and $(Ne^{20}, 6n$ or $7n)$ reactions suggests that Ar^{40} deposits, on the average, about the same angular momentum spectrum as does Ne^{20}.

The new range data extend the experimental measurements for Dy ranges in Al to 60 MeV. This broad span allows a more direct comparison with range and stopping power information for fission fragments and other heavy nuclei.

II. EXPERIMENTAL METHODS

Separated isotopes of the following composition were obtained from the Isotope Sales Division, Oak Ridge National Laboratory: cadmium-114 (99.09% Cd^{114}, 0.07% Cd^{116}); cadmium-116 (97.2% Cd^{116}, 1.44% Cd^{114}). Targets were prepared by vacuum evaporation of $Cd^{114}F_2$ and $Cd^{116}F_2$ onto weighed Al discs. Target thicknesses of 30–50 $\mu g/cm^2$ were determined by weight. It is estimated that the uncertainty in determining the average target thickness by this method is $\pm 2\%$.

Stacks of these targets and various catcher foils were mounted on water-cooled copper blocks and irradiated with Ar^{40} beams from the Berkeley HILAC; the copper target assembly served as a Faraday cup. Irradiation energies for each target were calculated from the experimental range-energy curve of Sikkeland for Ar^{40} in Al.[7] The initial energy of the beam was taken to be 10.6 Mev/amu. The energies of the recoiling product nuclei were calculated from the following relationship for compound nucleus formation:

$$E_R = A_b A_R E_b / (A_b + A_T)^2, \qquad (1)$$

† Work supported by the U. S. Atomic Energy Commission.
* A. P. Sloan Fellow.
[1] J. M. Alexander and D. H. Sisson, Phys. Rev. 128, 2288 (1962).
[2] G. N. Simonoff and J. M. Alexander, Phys. Rev. 133, B104 (1964).
[3] J. M. Alexander and G. N. Simonoff, Phys. Rev. 133, B93 (1964).
[4] J. M. Alexander, J. Gilat, and D. H. Sisson, Phys. Rev. 136, B1289 (1964).
[5] J. M. Alexander and G. N. Simonoff, Phys. Rev. 162, 952 (1967).
[6] H. Kumpf and V. A. Karnaukhov, Zh. Eksperim. i Teor. Fiz. 46, 1545 (1964) [English transl.: Soviet Phys.—JETP 19, 1045 (1964)].

[7] T. Sikkeland, Lawrence Radiation Laboratory Report No. UCRL-16453, 1965 (unpublished).

where E_R is the energy of the recoiling nucleus, E_b is the energy of the incident projectile, A_R is the mass of the recoiling nucleus, A_b is the mass of the projectile, and A_T is the mass of the target nucleus.

The recoiling reaction products from the thin targets were stopped in Al catcher foils placed downstream in the stack. In most of the cross-section measurements, the recoils were stopped in a single Al foil of 1.1–2.5 mg/cm². In those experiments in which differential range information was sought, the recoiling nuclei usually traveled over half the recoil distance in a single Al foil (typically ≈ 1.7 mg/cm²) and then were stopped in 6–10 Al leaves of ≈ 150 μg/cm² thickness. These leaves were inspected visually and found to be free from pin holes. To determine the contribution of foil inhomogeneities to the measured straggling, experiments were performed in which the entire path of the recoils was through Al leaf. These results are discussed in Sec. III.

Following the irradiation, the α activity in each catcher was measured by 2π methane-flow proportional counters. Typically the α activity was observed for 16 h following the irradiation. The resultant decay curves of each foil were subjected to a least-squares analysis (the CLSQ code of Cumming).[8] The cross sections for production of Dy¹⁵¹, Dy¹⁵⁰, and Tb¹⁴⁹ were determined from the activities at the end of the irradiation. For this purpose, the α branching was taken to be 5.9% for Dy¹⁵¹, 18% for Dy¹⁵⁰, and 22.6% for Tb¹⁴⁹ᵍ.[9,10] It is reasonably clear that essentially all the Tb¹⁴⁹ observed in these experiments comes from decay of Dy¹⁴⁹; cross sections for Dy¹⁴⁹ are estimated to be about six times as large as we report for Tb¹⁴⁹.[3,10]

The average projected range $\bar{R}_{||}$ and the range-straggling parameter were determined from plots of the cumulative activities versus cumulative thickness of Al traversed.[11] One-half the thickness of the CdF₂ target was included and multiplied by 0.583 to convert to μg/cm² of Al equivalent. Some of the Tb¹⁴⁹ range values were determined by measurement of the average depth of imbeddedness in a rather thick Al foil. In this method, the catcher foils of 1.1 to 2.5 mg/cm² were turned over between successive counts so that two different decay curves were obtained. Thus the intensity of emitted α particles was measured from each side of the foil.

At a particular time the activities, A_1 and A_2, were observed from the two sides of the foil of thickness T. Then we have

$$A_1/A_2 = (1 - t_1/R_\alpha)/(1 - t_2/R_\alpha), \qquad (2)$$

where R_α is the effective range of the α particles

[8] J. B. Cumming, U. S. Atomic Energy Commission Report No. NASNS 3107, 1962, p. 25 (unpublished).

[9] R. D. Macfarlane and D. W. Seegmiller, Nucl. Phys. **53**, 449 (1964).

[10] Y. Y. Chu, E. M. Franz, and G. Friedlander, Phys. Rev. **175**, 1523 (1968).

[11] L. Winsberg and J. M. Alexander, Phys. Rev. **121**, 518 (1961).

TABLE I. Cross-section results.

E_b (lab) (MeV)	Cross section (mb)		
	Dy¹⁵¹	Dy¹⁵⁰	Tb¹⁴⁹
Cd¹¹⁴+Ar⁴⁰→Dy¹⁵⁴*			
239.5			0.070
216.5		1.32	2.2
196.5	1.07	5.43	20.5
191		34.1	19.3
173		123	29.5
170	15.9	143	20.0
160	20.4	142	16.8
156		89.8	9.2
141	3.4	13.0	0.30
Cd¹¹⁶+Ar⁴⁰→Dy¹⁵⁶*			
285			0.032
271			1.70
261		0.17	1.13
256		1.31	2.52
254			1.80
244			6.41
240		6.33	13.3
227.5		32.5	33.4
220.5	1.75		30.5
212		90.9	32.3
212		117	
210	8.93		32.6
204	44.8		26.4
197	90.6	154	22.5
177	126	153	5.68
171	148	111	4.03
157		16.1	

being measured and t_1 and t_2 are the average depths from the surface to the radioactive nuclei.

Since $T = t_1 + t_2$, it follows that if R_α is known and A_1 and A_2 measured, the average distance of penetration of the recoil nuclei into the catcher can be determined and thus $\bar{R}_{||}$ can be obtained. It should be noted that if $t_1 = t_2$, the value of R_α used has no effect on the determination. In general, however, $t_1 \neq t_2$ and the calculated range $\bar{R}_{||}$ is somewhat sensitive to the choice of R_α. A value of 4.14 mg/cm² of Al was used for R_α. This value was obtained by observing the α activity from both sides of a foil in which the average depth of the α-emitting nuclei was already known from differential-range experiments. Alexander and Simonoff[12] obtained a value of 4.04 mg/cm² in similar experiments.

III. RESULTS

A. Excitation Functions

The cross sections for (Ar⁴⁰, xn) reactions with Cd¹¹⁴ and Cd¹¹⁶ are presented in Table I. In Figs. 1 and 2, these data, expressed as a fraction of the total

[12] J. M. Alexander and G. N. Simonoff, Phys. Rev. **130**, 2383 (1963).
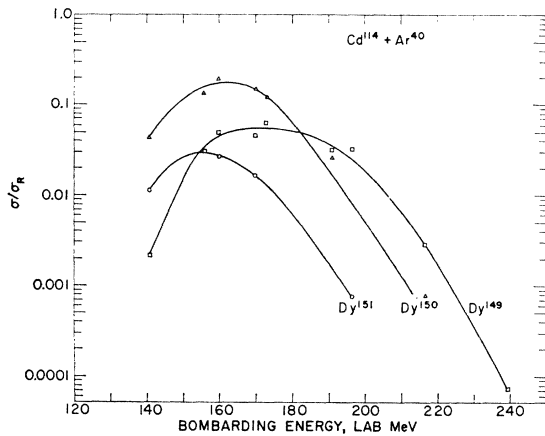
FIG. 1. Fraction of the total reaction cross section σ/σ_R versus bombarding energy for $Cd^{114}+Ar^{40}$.

reaction cross section σ/σ_R, are shown as a function of excitation energy. For this purpose a systematic extrapolation of the calculations of σ_R by Thomas[13] has been used. These values of σ_R are very close to those obtained from the classical sharp-cutoff approximation

$$\sigma_R = \pi R^2(1 - V/E_{c.m.}), \qquad (3)$$

where R is the sum of the target and projectile radii (radius parameter of 1.5 F), V is the Coulomb barrier, and $E_{c.m.}$ is the c.m. energy. In Figs. 3–5, the data for the (Ar^{40}, $5n$, $6n$, and $7n$) reactions are compared with the analogous reactions involving other projectiles. For this purpose, the values of σ/σ_R for the Ar^{40}-induced reactions have been normalized at the peak of the excitation function to the smooth curves obtained from the other reactions. It appears that the excitation functions for the Ar^{40}-induced reactions may be slightly wider than those for the lower-mass projectiles. This small effect might be the
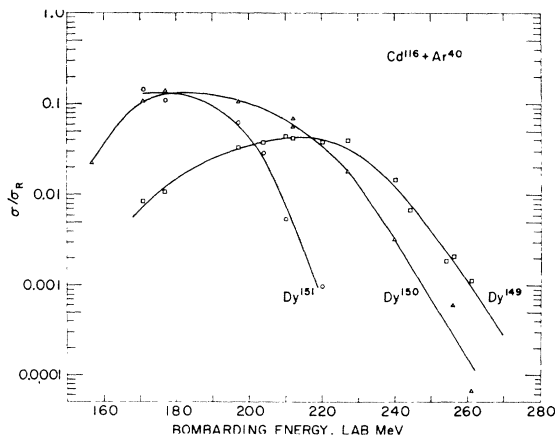
FIG. 2. Fraction of the total reaction cross section σ/σ_R versus bombarding energy for $Cd^{116}+Ar^{40}$.

[13] T. D. Thomas, Phys. Rev. 116, 703 (1959).
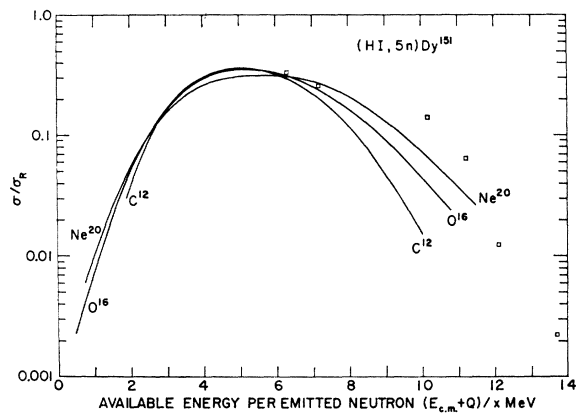
FIG. 3. Fraction of the total reaction cross section σ/σ_R versus available energy per emitted neutron for (HI, $5n$)Dy^{151} reactions. Smooth curves are from C^{12}, O^{16}, and Ne^{20} reactions reported in Ref. 3. Data points are from this work for Ar^{40}.

result of energy spread of the Ar beam as discussed below.

It is clear in Figs. 3–5 that the magnitudes of σ/σ_R at the peaks of the excitation functions are very similar for C, N, O, and Ne projectiles. However, the cross sections for Ar^{40} had to be multiplied by a factor of 2.2–2.7 in order to normalize at the peak cross sections. This comparison can be made somewhat more quantitative by estimation of the fraction f_n of reactions involving only neutron and γ-ray emission. For Cd^{116} f_n is estimated to be 0.34 at 77 MeV of excitation energy. This f_n value can be compared with 0.64 for projectiles of C^{12} to Ne^{22}.[3]

If we consider Dy^{156} excited to 77 MeV, and if we make the sharp-cutoff approximation as described above, then the reaction $Ne^{20}+Ba^{136}$ leads to $\langle J\rangle=42$ and $Ar^{40}+Cd^{116}$ leads to $\langle J\rangle=54$. It is probable however that the (HI, xn) reactions arise from the states of lowest angular momentum. That is, the noncompound nucleus reactions may occur at the highest
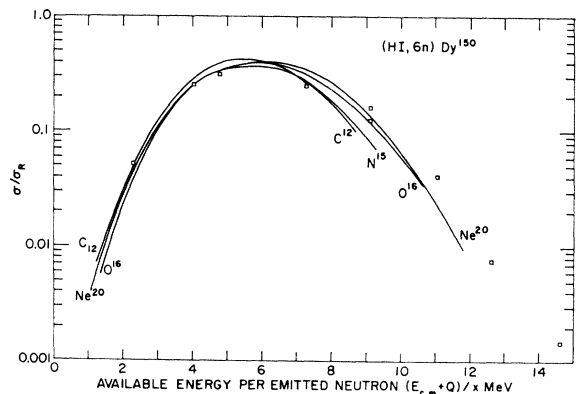
FIG. 4. Fraction of the total reaction cross section σ/σ_R versus available energy per emitted neutron for (HI, $6n$)Dy^{150} reactions. Smooth curves are from C^{12}, N^{15}, and Ne^{20} reactions reported in Ref. 3. Data points are from this work for Ar^{40}.

TABLE II. Range measurements in Al.

Bombarding energy E_b (lab) (MeV)	Observed product	Recoil energy, E_R (MeV)	Average range, $\bar{R}_{||}$ (mg/cm²)	Measured straggling parameter, ρ_m	Corrected straggling parameter, ρ_s	Theoretical straggling parameter
		Differential-range data Cd¹¹⁶+Ar⁴⁰				
254	Dy¹⁴⁹	62.2	2.59	0.075	0.045	0.055
246	Dy¹⁴⁹	60.3	2.51	0.072	0.041	0.057
212	Dy¹⁴⁹	51.9	2.35	0.104[a]	0.071	0.059
212	Dy¹⁵⁰	52.3	2.34	0.105[a]	0.072	0.059
212	Dy¹⁴⁹	51.9	2.34	0.090	0.069	0.059
212	Dy¹⁵⁰	52.3	2.36	0.085	0.063	0.058
		Cd¹¹⁴+Ar⁴⁰				
160	Dy¹⁴⁹	40.2	2.02	0.101	0.087	0.066
160	Dy¹⁵⁰	40.5	2.03	0.104	0.090	0.066
156	Dy¹⁵⁰	39.5	1.96	0.101	0.088	0.068
156	Dy¹⁵⁰	39.5	1.99	0.098	0.085	0.067
		Range data from imbeddedness determinations				
		Cd¹¹⁶+Ar⁴⁰				
256	Dy¹⁴⁹	62.7	2.55			
227.5	Dy¹⁴⁹	55.7	2.39			
220.5	Dy¹⁴⁹	54.0	2.55			
210	Dy¹⁴⁹	51.4	2.32			
		Cd¹¹⁴+Ar⁴⁰				
216.5	Dy¹⁴⁹	54.4	2.61			
196.5	Dy¹⁴⁹	49.4	2.14			
185	Dy¹⁴⁹	46.5	2.29			
173	Dy¹⁴⁹	43.5	2.18			
170	Dy¹⁴⁹	42.7	1.97			

[a] All stopping foils used in these experiments were Al leaf of ≈ 170 μg/cm². In the other experiments one foil of ≈ 1.7 mg/cm² was used followed by Al leaves.

impact parameters and/or those compound nuclei of highest angular momenta may deexcite by charged-particle emission. With this assumption [namely, $\langle J \rangle_{min} = f_n^{1/2} \langle J \rangle$], one can calculate the minimum average angular momentum of the compound nuclei leading to (HI, xn) products $\langle J \rangle_{min}$. We calculate that $\langle J \rangle_{min}$ equals 33 for (Ne²⁰, xn) reactions and 31 for (Ar⁴⁰, xn) reactions, or essentially the same within the uncertainties. From this estimate we see that it is certainly possible that Ar⁴⁰ and Ne²⁰ lead to very similar angular momentum distributions in the compound nucleus Dy¹⁵⁶.

In a similar study, Kumpf and Karnaukhov[6] obtained excitation functions which, compared to our results, are significantly broader and are peaked at higher cross-section values and higher energies. Therefore they estimate a considerably larger value of $\langle J \rangle$ for the reactions of Ar⁴⁰ with Cd. We believe that this discrepancy arises from the inherent uncertainties in the energy and intensity of internal cyclotron beams. It should be pointed out here that neither the average energy nor the energy spread of Ar⁴⁰ beams is as well known as is that of lighter ions. Beam

handling from the Berkeley HILAC is usually such that the beam has an average energy of 10.4±0.2 MeV/amu. Obviously an uncertainty of ±0.2 MeV/amu is twice as serious for Ar⁴⁰ as for Ne²⁰. For these experiments we have reason to take 10.6 MeV/amu as the average beam energy, and we suspect that the energy spread of the beam makes some contributions to the width of the excitation functions. The only correction that we have made for this effect is to reject those cross sections near the energetic threshold for the reaction. The accelerator parameters are such that 10.6 MeV/amu is the highest average energy which one can expect. Therefore we feel that the bombarding energies given in Tables I and II cannot be too small.

B. Range Data

The average ranges and range straggling parameters are presented in Table II. Note in particular that at 212-MeV bombarding energy, the experiments in which the stopping was entirely in Al leaf give ρ values of 0.104±0.005 and 0.105±0.005 for Dy¹⁴⁹ and for Dy¹⁵⁰, while the experiments in which most of the stopping
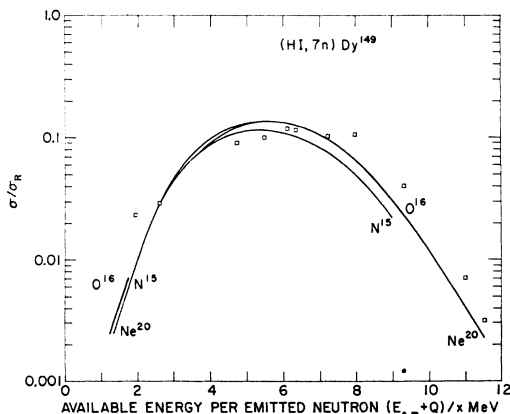
FIG. 5. Fraction of the total reaction cross section σ/σ_R versus available energy per emitted neutron for (HI, $7n$) Dy[149] reactions. Smooth curves are from N[14], O[16], and Ne[20] reactions reported in Ref. 3. Data points are from this work for Ar[40].

was in a single foil give ρ values of 0.090±0.005 and 0.085±0.005 for Dy[149] and Dy[150], respectively. We expect that the range distributions should be the same in the two different experiments provided that all foils are homogeneous. That they are significantly different probably results from inhomogeneities in the Al leaf. We can evaluate the average straggling contribution from the leaf alone by attributing the difference in the two experimental results to the extra leaves in the experiment in which the stopping was totally in Al leaf. If we assume that the various contributions to the straggling add in quadrature we find that for each leaf i the root-mean-square contribution to the straggling $_i\rho_f$ (from inhomogeneities) is 0.016± 0.006. We can use this result to correct the measured straggling parameters ρ_m as follows:

$$\rho_m{}^2 = \sum_i \rho_f{}^2 + \rho_w{}^2 + \rho_n{}^2 + \rho_s{}^2, \qquad (4)$$

where the subscripts w, n, and s refer to the contributions from the finite target thickness w, the nuclear reaction n, and the stopping effects s. We have used the equations and the systematic data given in Refs. 1 and 2 to estimate ρ_n and ρ_w. We have obtained ρ_s by subtraction, and the values are given in Table II. The theoretical estimates[14] of ρ_s are about 20% smaller than our results. The most important effect in the correction of ρ_m to ρ_s is that due to foil inhomogeneities ($\sum_i \rho_f{}^2$). The magnitude of this correction is about 25% for these measurements and would be about 1–5% if applied to the ρ values of Ref. 1.

All the range data are given in Table II. In Fig. 6 the new differential-range measurements obtained in the Ar[40] experiments are plotted against the recoil energies calculated from Eq. (1). The ranges measured by imbeddedness (not plotted) scatter considerably more than the differential ranges. Even so,

[14] J. Lindhard, M. Scharff, and H. E. Schiott, Kgl. Danske Videnskab. Selskab, Mat.-Fys. Medd. **33**, No. 14 (1963).

we find that if a least-squares fit is made to the previously reported range data,[1] combined with the differential-range data of this paper, the average deviation of the imbeddedness ranges from the smooth curve is only 4%. In Fig. 6 we show this least-squares fit to all the Dy range data

$$\bar{R}_{||} = -6.37 \times 10^{-3} + 9.34 \times 10^{-2} E - 2.32 \times 10^{-3} E^2$$
$$+ 4.26 \times 10^{-5} E^3 - 3.03 \times 10^{-7} E^4,$$

$$\text{for } 4 < E < 60 \text{ MeV} \qquad (5)$$

where $\bar{R}_{||}$ is expressed in mg/cm^2 and E in MeV. The new data reported in this paper are on an extension of the smooth curve through the previously reported data.[1] We take this over-all consistency as evidence that total momentum transfer occurs in the (Ar[40], xn) reactions as in the other (HI, xn) reactions. This evidence supports the conclusion that the mechanism for the (Ar[40], xn) reactions is compound-nucleus formation followed by neutron evaporation.

C. Correlations of Range-Energy Data

Consider a nucleus of energy E, range R, mass M_1, and nuclear charge Z_1 stopped in a medium of atomic mass M_2 and nuclear charge Z_2. In the theory of Lindhard, Scharff, and Schiott[14] (LSS), the energy E of the moving ion may be expressed in terms of the dimensionless parameter ϵ,

$$\epsilon = a M_2 E / Z_1 Z_2 e^2 (M_1 + M_2). \qquad (6)$$

The range R may be expressed in terms of the di
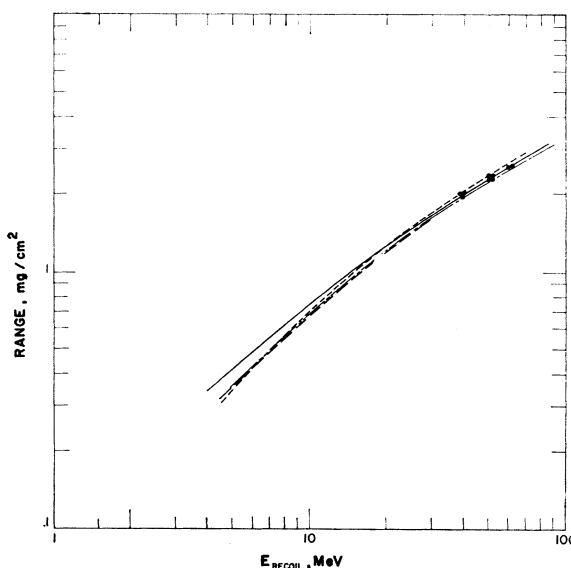
FIG. 6. Range-energy curves for Dy[149] in Al. Data points are from this work. The solid curve is a least-squares fit to all Dy[149] data from Ref. 1 and this work. The other curves are as follows: long-dashed-short-dashed line from Schilling and Northcliffe (Ref. 17); short-dashed line from Aras, Menon, and Gordon (Ref. 16); long-dashed line from Steward (Ref. 15).

mensionless parameter ρ,

$$\rho = RNM_2 4\pi a^2 M_1 (M_1 + M_2)^{-2}, \qquad (7)$$

where $a = 0.8853(\hbar^2/me^2)(Z_1^{2/3} + Z_2^{2/3})^{1/2}$ is the Thomas-Fermi screening length, e is the electron mass, and N is the atomic density of the stopping medium.

The total energy loss $(d\epsilon/d\rho)$ is given as the sum of contributions from nuclear and electronic stopping,

$$(d\epsilon/d\rho) = (d\epsilon/d\rho)_n + (d\epsilon/d\rho)_e. \qquad (8)$$

The total dimensionless range $\rho(\epsilon)$ can be expressed as a combination of the dimensionless range for electronic stopping $\rho_e(\epsilon)$ and a correction for nuclear stopping $\Delta(K, \epsilon)$,

$$\rho(\epsilon) = \rho_e(\epsilon) - \Delta(K, \epsilon), \qquad (9)$$

where

$$\rho_e(\epsilon) = 2K^{-1}\epsilon^{1/2} \qquad (10)$$

and

$$K = \xi \frac{0.0793 Z_1^{1/2} Z_2^{1/2} (M_1 + M_2)^{3/2}}{(Z_1^{2/3} + Z_2^{2/3})^{3/4} M_1^{3/2} M_2^{1/2}}, \qquad \xi \simeq Z_1^{1/6}. \qquad (11)$$

In Fig. 6 we show the results of three different semi-empirical calculations of the range-energy curve for Dy^{149} in Al. The calculation of Steward[15] is based on the adjustment of the LSS parameters to fit available data on fission fragments and Ar ions.

The calculation following Aras, Menon, and Gordon[16] is based on adjustment of ξ to a value of $Z_1^{0.212}$ and $\Delta(K, \epsilon)$ values from Ref. 14. The calculation by Schilling and Northcliffe is based on extrapolation of stopping powers with ion velocity and ion mass.[17] At low velocities, the LSS theory is employed to make nuclear-stopping corrections.[14]

Several authors have pointed out the attractiveness of correlating experimental stopping-power data for many different ions in terms of empirical charge and ionization parameters.[18] Recently, Cumming and Crespo[19] and Pierce and Blann[20] have used this approach for the Bethe-Bloch stopping power equation for electronic stopping:

$$(dE/dR)_e = 4\pi N e^4 Z_{\text{eff}}^2 Z_2 M_2^{-1} V^{-2} \ln(2mV^2 I^{-1}), \qquad (12)$$

where N is the atomic density and the logarithmic term depends on ion velocity V and the ionization

parameter I characteristic of the stopping medium. One treats the charge Z_{eff}^2 as an empirical parameter (the effective charge $Z_{\text{eff}} = \gamma Z_1$). The ratio of electronic stopping power for a heavy ion $(dE/dR)_{e,M_1,Z_1}$ to the stopping power for the proton $(dE/dR)_p$ of the same velocity gives the value of

$$\frac{(dE/dx)_{e,M_1,Z_1}}{(dE/dx)_p} = \frac{\gamma^2 Z_1^2}{\gamma_p^2}. \qquad (13)$$

The effective charge of the proton, γ_p, has been empirically determined from Eq. (12) and stopping-power measurements.[21,22] To compare different recoil ions, one examines the fractional effective charge γ as a function of the reduced velocity V_R $(V_R = V\hbar/e^2 Z_1^{2/3})$.

We have differentiated Eq. (5) to obtain total dE/dR (or dE/dx) values as a function of energy. These values of dE/dx have been corrected for nuclear stopping by employing the theoretical values[14] of $(d\epsilon/d\rho)_n$ for $\epsilon < 10$ and the following asymptotic formula[20] for $\epsilon > 10$:

$$(d\epsilon/d\rho)_n = (2\epsilon)^{-1} \ln(1.294\epsilon), \qquad \text{for } \epsilon > 10. \qquad (14)$$

We have calculated γ for the Dy ions as a function of reduced velocity from Eq. (13).[21,22]

In Fig. 7 we show the values of γ for several different systems. Values for stopping in Al are shown for Dy^{149} from our own results along with those for Br^{79,80}, I^{127,19,23} and fission fragments.[24] As shown in the figure these values of γ correlate very well with one another and they could be easily fit by a single curve. As suggested by others[19,20] one can reverse the above procedure and use Fig. 7 to calculate $(dE/dR)_e$ for other heavy ions. The addition of $(dE/dR)_n$ followed by integration can lead to a range-energy curve for any ion in Al. A range-energy curve generated in this way is, of course, quite sensitive to the relationship used for γ. Also shown in Fig. 7 are values of γ obtained by Pierce and Blann[20] for the stopping of Br^{79} and I^{127} in He and Kr, as well as the variation of γ with V_r for fission fragments in mylar as obtained by Cumming and Crespo.[19] The data of Ref. 20 agree quite well with our data below $V_r = 0.3$. Above that point, the values of γ derived by Pierce and Blann are consistent with the relationship $\gamma = [1 - \exp(-0.95 V_r)]$ and appear to be somewhat higher than the values derived from aluminum. This might represent experimental errors. The deviation of the Mylar data of Cumming and Crespo from the other data may result from their approximation for the proton-stopping powers in Mylar. We conclude that below $V_r = 0.3$, reliable predictions of stopping powers and range for a wide range of stopped ions can be made using the data

[15] P. G. Steward, Lawrence Radiation Laboratory Report No. UCRL-18127, 1968 (unpublished).

[16] N. K. Aras, M. P. Menon, and G. E. Gordon, Nucl. Phys. **69**, 337 (1965).

[17] R. Schilling and L. Northcliffe (private communication).

[18] W. H. Barkas, in *Nuclear Research Emulsions*, edited by W. H. Barkas (Academic Press Inc., New York, 1963), Vol. I; H. H. Heckman, E. L. Hubbard, and W. G. Simon, Phys. Rev. **129**, 1240 (1963); H. H. Heckman, B. L. Perkins, W. G. Simon, F. M. Smith, and W. H. Barkas, *ibid.* **117**, 544 (1960); W. Booth and I. S. Grant, Nucl. Phys. **63**, 481 (1965); P. G. Roll and F. E. Steigert, *ibid.* **16**, 534 (1960); **17**, 54 (1960); Phys. Rev. **120**, 470 (1960); L. C. Northcliffe, Ann. Rev. Nucl. Sci. **13**, 67 (1963).

[19] J. B. Cumming and V. Crespo, Phys. Rev. **161**, 287 (1967).

[20] T. E. Pierce and M. Blann, Phys. Rev. **173**, 390 (1968).

[21] W. Whaling, in *Handbuch der Physik*, edited by S. Flügge (Springer-Verlag, Berlin, 1958), 5th ed. Vol. 34, p. 193.

[22] T. Hall, Phys. Rev. **79**, 504 (1950).

[23] C. D. Moak and M. D. Brown, Phys. Rev. **149**, 244 (1966).

[24] R. B. Leachman and H. W. Schmitt, Phys. Rev. **96**, 1366 (1954); J. M. Alexander and M. F. Gazdik, *ibid.* **120**, 874 (1960).
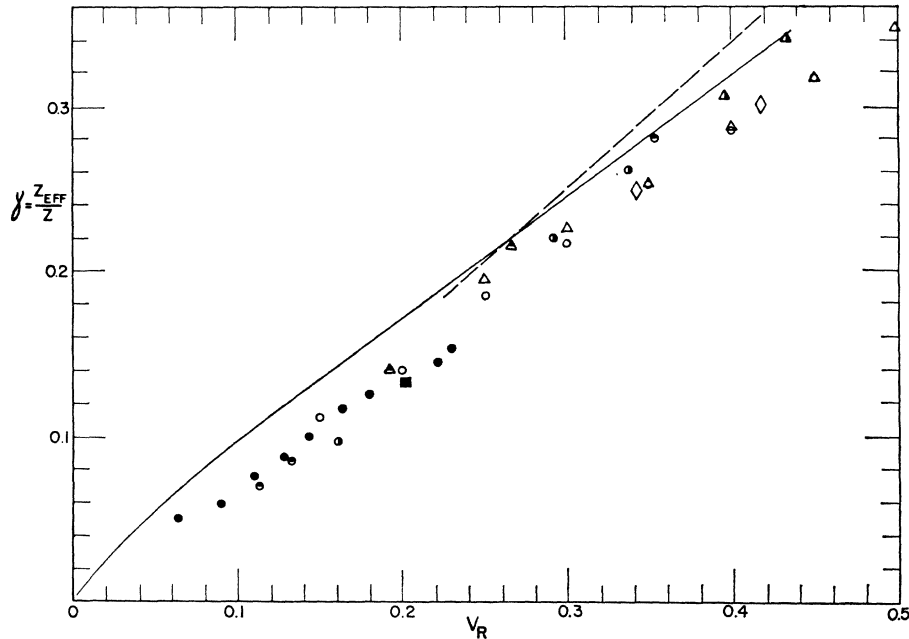
FIG. 7. Fractional effective charge $\gamma = Z_{eff}/Z_1$ versus reduced velocity for various ions in Al, He, and Kr. The data points are indicated as follows: In aluminum Dy^{149} ●, I^{127} ○, $Br^{79,81}$ △, median heavy fission fragment □, median light fission fragment ◇; in $HeBr^{79}$ ▲, I^{127} ◐; in $KrBr^{79}$ ▲, I^{127} ◓. The dashed line is for fission products stopped in Mylar as obtained in Ref. 19. The solid line is the line $\gamma = [1 - \exp(-9.95\ V_r)]$.

of Fig. 7.[25] The applicability of such a "universal curve" to the prediction of stopping powers and ranges for medium to heavy mass ions above $V_r = 0.3$ is yet untested.

IV. CONCLUSIONS

Our cross-section data indicate that the average angular momentum leading to $Dy^{149,150,151}$ products in $(Ar^{40}, 6n$ and $7n)$ reactions is not very different from the same quantity in $(Ne^{20}, 6n$ and $7n)$ reactions. It is not possible to discern in the present experiment whether this is mainly the result of a reduced probability for formation of a compound nucleus or the result of increased probability of deexcitation by

charged-particle emission from the compound nuclei produced.

The new range data extend experimental range-energy information to 60 MeV. These data, expressed in terms of fractional effective change, are found to be consistent with data for other heavy species stopped in Al. This effective charge curve can now be employed to calculate "electronic stopping powers" for other heavy ions.

ACKNOWLEDGMENTS

[25] *Note added in proof.* The recent paper of R. Kalish *et al.* [Phys. Rev. **183**, 431 (1969)] presents data for the stopping of Ta ions in C, Al, Ag, and Au. The data plotted in Fig. 4 of that paper supports our conclusion.